Available online at www.sciencedirect.com
ScienceDirect
Catalysis Communications 8 (2007) 237–240
CATALYSIS COMMUNICATIONS
www.elsevier.com/locate/catcom

Mn-substituted Ca–La–hexaaluminate nanoparticles for catalytic combustion of methane

Shunqing Li [a,b], Haitao Liu [a,b], Liang Yan [a], Xiaolai Wang [a,*]

[a] State Key Laboratory for Oxo Synthesis and Selective Oxidation, Lanzhou Institute of Chemical Physics, Chinese Academy of Sciences, Lanzhou 730000, PR China

[b] The Graduate University of the Chinese Academy of Sciences, Beijing 10039, PR China

Received 4 November 2005; received in revised form 23 May 2006; accepted 29 May 2006
Available online 6 June 2006

Abstract

Mn-substituted Ca–La–hexaaluminate rod-like nanoparticles ($Ca_{1-x}La_xMnAl_{11}O_{19-\alpha}$) with high surface area ranging from 47 to 80 m^2/g for catalytic combustion of methane have been prepared using alumina sol as the $(NH_4)_2CO_3$ coprecipitation precursor and a supercritical drying (SCD) method. Ca substitution gave rise to the maximum combustion activity ($T_{10\%} = 459$ °C) at $x = 0$ owing to the highest surface area. Meanwhile, Ca substitution affects the oxygen sorption property and the oxidation state of Mn ions in the hexaaluminate lattice. $Ca_{0.6}La_{0.4}MnAl_{11}O_{19-\alpha}$ catalyst with high catalytic activities was obtained owing to the excellent performance of activating oxygen.

Keywords: Ca–La–hexaaluminate; Catalytic combustion; Nanoparticle; Methane

1. Introduction

Hexaaluminate materials are attractive as combustion catalysts for gas turbine applications, due to the high thermal stability associated with their peculiar layered structure that consists of γ-Al_2O_3 spinel block intercalated by planes (mirror planes) in which the largest cations are located [1–4]. The large cation plays an important role on the catalytic activity and thermal stability. Several compositions have been investigated [5–7]. Nevertheless, La–Ca composition has been rarely reported, hence further research on the catalysts is necessary.

Since hexaaluminate with high catalytic activities were prepared by adopting reverse microemulsion-mediated synthesis method [8–10], much attention has been paid to synthesis of with high surface area. We attempt to develop a practical and cost-effective synthesis method to prepare mesoporous catalysts with high surface areas. The hexaaluminate-based catalysts have been prepared using alumina sol [11] as the $(NH_4)_2CO_3$ coprecipitation precursor and a supercritical drying (SCD) method [12].

In this report, $Ca_{1-x}La_xMnAl_{12}O_{19-\alpha}$ ($x = 1$, 0.8, 0.6, 0.4, 0.2, 0) hexaaluminate nanoparticles were prepared and the catalytic activities for methane combustion were investigated. Moreover, N_2-adsorption, X-ray diffraction (XRD), TEM, temperature programmed reduction (TPR) of hydrogen and temperature programmed desorption (TPD) of oxygen were used to study the structural and morphological properties.

2. Experimental

2.1. Preparation of the catalysts [12,13]

Mn-substituted hexaaluminate-based catalysts have been prepared using alumina sol in place of aluminum nitrate as the $(NH_4)_2CO_3$ coprecipitation precursor and a supercritical drying (SCD) method. The mixed appropriate

* Corresponding author. Tel.: +86 931 8275 727; fax: +86 931 8277 787.
E-mail address: lishunqing2003@yahoo.com.cn (X. Wang).

1566-7367/$ - see front matter © 2006 Elsevier B.V. All rights reserved.
doi:10.1016/j.catcom.2006.05.039

amounts of manganese, lanthanum, calcium nitrates and alumina sol solution was poured into a well-stirred container with an ammonium carbonate solution at 60 °C to form the hexaaluminate precursor precipitate. The slurry was aged for 10 h at 60 °C, and then filtered, and washed with distilled water. The filter cake was then dried under supercritical conditions of ethanol (260 °C, 8.0 MPa). Finally, the aerogel was calcined in a muffled furnace at 1200 °C for 5 h in air.

2.2. Catalyst characterization

The surface area and the pore size distribution of the different catalysts were determined by nitrogen adsorption at 77 K on a Micrometrics ASAP 2010 instrument. The surface area was determined according to the Brunauer–Emmett–Teller theory and the analysis of the diameter and the hole volume were carried out.

The crystal phases of the various catalysts were detected by X-ray diffraction, on a Shimadzu Diffractometer XD-3A.The operation parameters were: Cu Kα radiation, Ni filter, 30 mA, 40 kV, 2θ scanning from 5° to 80° with the scanning speed of 4°/min.

The morphology and size of the catalysts were studied using a transmission electron microscopy (HITACHI-8100IV) with a voltage of 200 kV. The test samples were prepared by its suspension on the copper net.

Temperature programmed reduction (TPR) of hydrogen was measured in a flow system. A known amount (50 mg) of sample was pretreated in an argon stream (35 ml/min) up to 300 °C for 30 min at a rate of 10 °C/min and subsequently cooled down to room temperature. Then a mixture of 10 vol% H_2 in Ar was admitted onto the samples and temperature was raised at a rate of 10 °C/min up to 920 °C. Hydrogen consumption amount was detected by a TCD.

Temperature programmed desorption (TPD) of oxygen was measured in the same apparatus. A known amount (50 mg) sample was pretreated in an oxygen stream (50 ml/min) at 800 °C for 1 h and subsequently cooled to room temperature. Then a helium stream (35 ml/min) was introduced into the system and temperature was raised at a constant rate of 10 °C/min up to 920 °C. Desorbed oxygen in the effluent gas was detected by the TCD.

2.3. Activity tests

The reaction of methane combustion was carried out in a conventional flow system under atmospheric pressure. Catalyst (0.8 ml) (20–40 mesh) was loaded in a quartz reactor (i.d. 10 mm), with quartz fiber packed at the end of the catalyst bed. A mixture gas of 4 vol% O_2 and 1 vol% CH_4 (nitrogen as balance) was fed into the catalyst bed at GHSV = 15,000 h^{-1}. The inlet and outlet gas compositions were analyzed by on-line gas chromatography with a packed column of carbon molecular sieve and a thermal conductivity detector.

3. Results and discussion

3.1. Surface area and pore size distribution

The surface area and pore volume as well as average pore diameter of the $Ca_{1-x}La_xMnAl_{11}O_{19-\alpha}$ catalysts are summarized in Table 1. The $Ca_{1-x}La_xMnAl_{11}O_{19-\alpha}$ catalysts with high surface area in the range between 47 and 80 m^2/g were obtained. The $CaMnAl_{11}O_{19-\alpha}$ catalyst possesses the highest surface area. The surface area changed with the replacement of Ca^{2+} with La^{3+}, probably due to the variation of the thickness of the planar crystals and the crystal size. Meanwhile, the average pore diameters varied from 66 to 80 Å, showing the introduction of large cation in the mirror plane has some effect on the structure of the internal pores inside the alumina network.

3.2. Crystalline phases

The XRD patterns of the $Ca_{1-x}La_xMnAl_{11}O_{19-\alpha}$ catalysts are shown in Fig. 1. The single hexaaluminate phases were formed when x varies from 0.2 to 1, while α-Al_2O_3 and alumina-rich magnetoplumbite hexaaluminate phases [JCPDS 83-0270] were observed in the crystalline phases of the $CaMnAl_{11}O_{19-\alpha}$ catalyst. The hexaaluminates tend to form with the replacement of Ca^{2+} with La^{3+}. It is obvious that higher valence can promote the formation of hexaaluminate more effectively. Meanwhile, the catalysts showed broad diffraction peaks, indicating the catalysts were composed of fine particles.

3.3. Microstructure analysis

Fig. 2 presents the TEM results of the catalysts. The catalysts are composed of rod-like particles, which are 5–20 nm in diameter and 50–150 nm in length. The dimension increases with the replacement of Ca^{2+} with La^{3+}, leading to the decrease of the surface area. Moreover, small amount of granular particles are observed, which probably correspond to the α-Al_2O_3 crystal. The results are consistent with those of the XRD analysis.

3.4. TPR measurements

The TPR profiles of the $Ca_{1-x}La_xMnAl_{11}O_{19-\alpha}$ catalysts are shown in Fig. 3. The main reduction peaks around 400 °C corresponds to the reduction of the Mn^{3+} ions

Table 1
The properties of the $Ca_{1-x}La_xMnAl_{11}O_{19-\alpha}$ catalysts

Catalyst	S_{BET} (m^2/g)	V_{pore} (cm^3/g)	d_{pore} (Å)
$CaMnAl_{11}O_{19-\alpha}$	79.5	0.139	70.1
$Ca_{0.8}La_{0.2}MnAl_{11}O_{19-\alpha}$	52.3	0.094	72.0
$Ca_{0.6}La_{0.4}MnAl_{11}O_{19-\alpha}$	70.7	0.117	66.2
$Ca_{0.4}La_{0.6}MnAl_{11}O_{19-\alpha}$	55.5	0.099	71.5
$Ca_{0.2}La_{0.8}MnAl_{11}O_{19-\alpha}$	47.2	0.082	69.9
$LaMnAl_{11}O_{19-\alpha}$	55.8	0.111	80.1

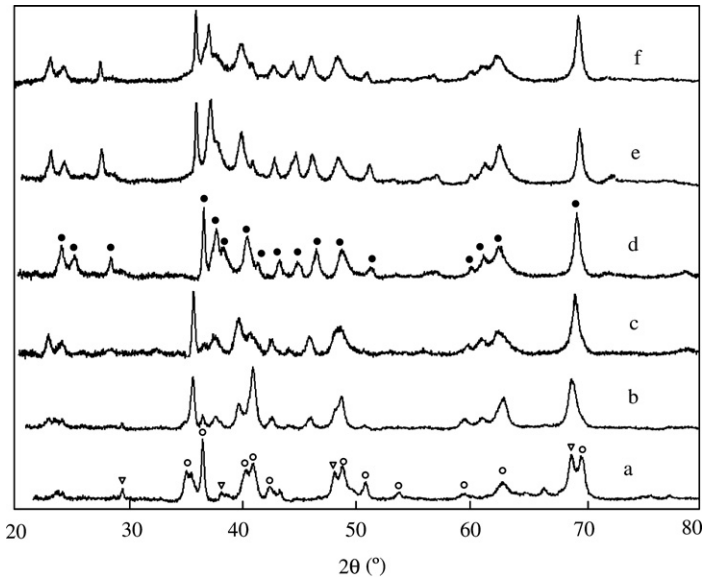

Fig. 1. XRD patterns of the $Ca_{1-x}La_xMnAl_{11}O_{19-\alpha}$ catalysts: (a) $x = 0$; (b) $x = 0.2$; (c) $x = 0.4$; (d) $x = 0.6$; (e) $x = 0.8$ and (f) $x = 1$; (●) La-hexaaluminate (○) $Ba_{0.717}Al_{11}O_{17.282}$ (▽) α-Al_2O_3.

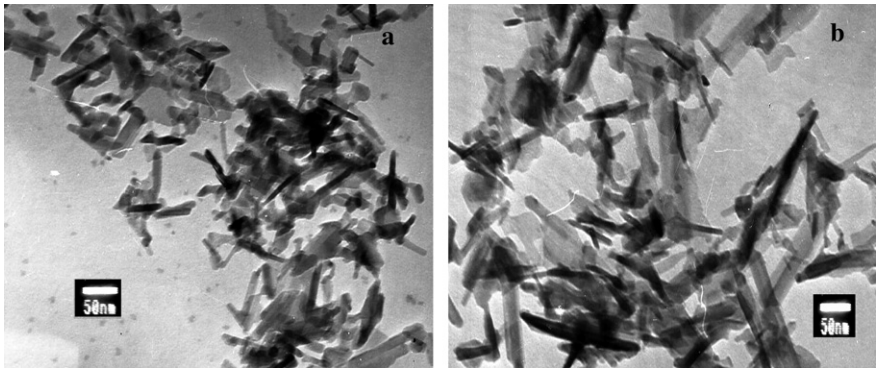

Fig. 2. TEM photographs of the catalysts: (a) $CaMnAl_{11}O_{19-\alpha}$ and (b) $Ca_{0.6}La_{0.4}MnAl_{11}O_{19-\alpha}$.

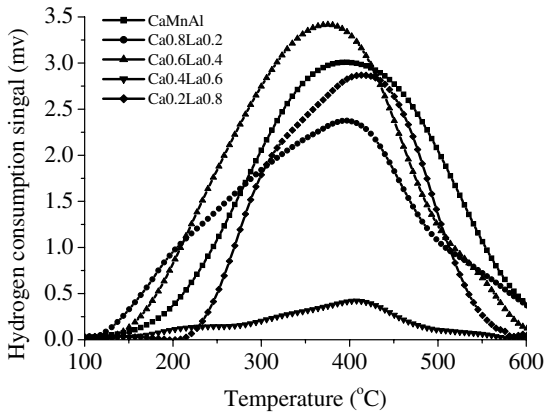

Fig. 3. TPR under hydrogen of the $Ca_{1-x}La_xMnAl_{11}O_{19-\alpha}$ catalysts.

locating in an Al interstitial site near the mirror plane, which is attributed to the most reactive Mn species [14,15]. The lowest temperature and maximum area are present for the $Ca_{0.6}La_{0.4}MnAl_{11}O_{19-\alpha}$ catalyst, showing the catalyst possesses the highest ability of activating oxygen and Mn^{3+} content. On the contrary, the highest temperature and minimum area are for the $Ca_{0.4}La_{0.6}MnAl_{11}O_{19-\alpha}$ catalyst, showing the lowest ability of activating oxygen and Mn^{3+} content.

3.5. O_2-TPD

TPD profiles of oxygen from the $Ca_{1-x}La_xMnAl_{11}O_{19-\alpha}$ catalysts are shown in Fig. 4. Two main desorption peaks around 150 °C and 750 °C are present. The first peak probably corresponds to physically adsorbed oxygen on the catalyst surface, while the latter corresponds to the lattice oxygen. Arai concluded that oxygen species desorbed at high temperature are related to the oxidation/reduction of Mn ion [5]. From the difference of the peak location and area, it is inferred that the nature of the large cation in the mirror plane can affect the activity and the content of lattice oxygen. When compared to the peak location of the $Ca_{1-x}La_xMnAl_{11}O_{19-\alpha}$ catalysts, the lowest tempera-

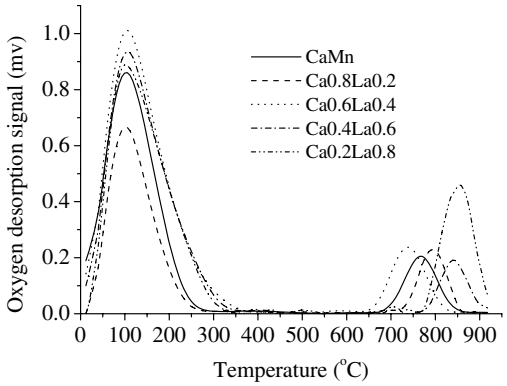

Fig. 4. TPD profiles of oxygen from the $Ca_{1-x}La_xMnAl_{11}O_{19-\alpha}$ catalysts.

ture is present for the $Ca_{0.6}La_{0.4}MnAl_{11}O_{19-\alpha}$ catalyst, showing that the $Ca_{0.6}La_{0.4}MnAl_{11}O_{19-\alpha}$ catalyst possesses the most active oxygen. Nevertheless, the smallest area is present for the $CaMnAl_{11}O_{19-\alpha}$ catalyst, showing the catalyst has lowest content of lattice oxygen. The results revealed that the content of the lattice oxygen increase with the replacement of Ca^{2+} with La^{3+}, probably due to the increased defectiveness in the hexaaluminate lattice.

3.6. Catalytic combustion of methane

The catalytic activities for methane combustion over the $Ca_{1-x}La_xMnAl_{11}O_{19-\alpha}$ catalysts are shown in Fig. 5. The catalysts were highly active except the $LaMnAl_{11}O_{19-\alpha}$ catalyst. The $T_{10\%}$, $T_{50\%}$ and $T_{90\%}$ corresponding to 10%, 50%, and 90% conversion are reported in Table 2. The lowest ignition temperature ($T_{10\%}$) and the lowest complete conversion of methane temperature ($T_{90\%}$) were obtained at $x = 0$, indicating the $CaMnAl_{11}O_{19-\alpha}$ catalyst possesses the highest catalytic activity owing to the highest surface area. Meanwhile, the $Ca_{0.6}La_{0.4}MnAl_{11}O_{19-\alpha}$ catalyst possesses the high catalytic activity owing to the best performance of activating oxygen. On the contrary, the $Ca_{0.4}La_{0.6}MnAl_{11}O_{19-\alpha}$ catalyst possesses the lowest catalytic activity due to the lowest ability of activating oxygen and content of lattice oxygen. From above, it can be concluded that the lattice oxygen plays an important role in catalytic reaction. The intrinsic activities of the $Ca_{1-x}La_xMnAl_{11}O_{19-\alpha}$ catalysts (mol CH_4 converted per hour and per square meter) are also given in Table 2 [16]. The maximum value was obtained at $x = 0.2$.

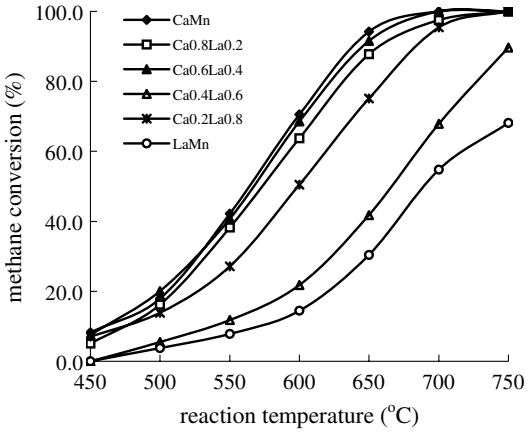

Fig. 5. Catalytic combustion of CH_4 over the $Ca_{1-x}La_xMnAl_{11}O_{19-\alpha}$ catalysts.

Table 2
Catalytic activity expressed as $T_{10\%}$, $T_{50\%}$ and $T_{90\%}$ in °C and as intrinsic activity (10^{-5} mol CH_4 converted per hour and per square meter)

Catalyst	$T_{10\%}$ (°C)	$T_{50\%}$ (°C)	$T_{90\%}$ (°C)	Intrinsic activity at 500 °C
$CaMnAl_{11}O_{19-\alpha}$	459	564	641	6.0
$Ca_{0.8}La_{0.2}MnAl_{11}O_{19-\alpha}$	472	573	661	8.2
$Ca_{0.6}La_{0.4}MnAl_{11}O_{19-\alpha}$	461	567	647	7.5
$Ca_{0.4}La_{0.6}MnAl_{11}O_{19-\alpha}$	536	666	750	2.6
$Ca_{0.2}La_{0.8}MnAl_{11}O_{19-\alpha}$	475	598	687	7.8
$LaMnAl_{11}O_{19-\alpha}$	565	690	820	1.8

4. Conclusions

Mn-substituted Ca–La–hexaaluminate rod-like nanoparticles with high surface area in the range between 47 and 80 m^2/g have been prepared using alumina sol as the $(NH_4)_2CO_3$ coprecipitation precursor and supercritical drying (SCD) method. The $CaMnAl_{11}O_{19-\alpha}$ catalyst possesses the highest catalytic activity owing to the highest surface area. The nature of the large cation in the mirror plane can affect the Mn^{2+}/Mn^{3+} redox process. The $Ca_{0.6}La_{0.4}MnAl_{12}O_{19-\alpha}$ catalyst with high catalytic activities was obtained owing to the excellent performance of activating oxygen.

References

[1] L.D. Pfefferle, W.C. Pfefferle, Catal. Rev. – Sci. Eng. 29 (1987) 219.
[2] M.F.M. Zwinkels, S.G. Järås, P.G. Menon, Catal. Rev. – Sci. Eng. 35 (1993) 319.
[3] H. Arai, H. Fukuzawa, Catal. Today 26 (1995) 217.
[4] Koichi Eguchi, Hiromichi Arai, Catal. Today 29 (1996) 379.
[5] M. Machida, K. Eguchi, H. Arai, J. Catal. 123 (1990) 477.
[6] G. Groppi, C. Cristiani, P. Forzatti, Catalysis 13 (1997) 85.
[7] Ben W.-L. Jang, R.M. Nelson, James J. Spivey, Meltem Ocal, R. Oukaci, George Marcelin, Catal. Today 47 (1999) 103.
[8] A.J. Zarur, J.Y. Ying, Nature 403 (2000) 65.
[9] A.J. Zarur, H.H. Hwu, J.Y. Ying, Langmuir 16 (2000) 3042.
[10] Prashant K. Sahu, B.D. Kulkarni, R.B. Khomane, S.A. Pardhy, U.D. Phalgune, P. Rajmohanan, Renu Pasricha, Chem. Commun. 15 (2003) 1876.
[11] Sung June Cho, Yong Seog Seo, Kwang Sup Song, Nam Jo Jeong, Sung Kyu Kang, Appl. Catal. B 30 (2001) 351.
[12] Junwei Wang, Zhijian Tian, Jinguang Xu, Yunpeng Xu, Zhusheng Xu, Liwu Lin, Catal. Today 83 (2003) 213.
[13] G. Groppi, M. Bellotto, C. Cristiani, P. Forzatti, P.L. Villa, Appl. Catal. A 104 (1993) 101.
[14] P. Artizzu-Duart, Y. Brullé, F. Gaillard, E. Garbowski, N. Guilhaume, M. Primet, Catal. Today 54 (1999) 181.
[15] M. Astier, E. Garbowski, M. Primet, Catal. Lett. 95 (2004) 31.
[16] P. Artizzu-Duart, J.M. Millet, N. Guilhaume, E. Garbowski, M. Primet, Catal. Today 59 (2000) 163.